

PAPER • OPEN ACCESS

Biocompatibility and degradation of the open-pored magnesium scaffolds LAE442 and La2

To cite this article: N Kleer-Reiter *et al* 2021 *Biomed. Mater.* **16** 035037

View the [article online](#) for updates and enhancements.



**BREATH
BIOPSY**

Breath Biopsy Panel for Focused Biomarker Discovery in Respiratory Disease Research

Providing high confidence identification of non-invasive breath biomarkers to distinguish, monitor and assess therapeutic responses across a range of chronic inflammatory airway diseases

WATCH OUR INTRODUCTORY WEBINAR

Biomedical Materials



PAPER

OPEN ACCESS

RECEIVED
7 July 2020

REVISED
17 March 2021

ACCEPTED FOR PUBLICATION
7 April 2021


PUBLISHED
21 April 2021

Original content from this work may be used under the terms of the [Creative Commons Attribution 4.0 licence](https://creativecommons.org/licenses/by/4.0/).

Any further distribution of this work must maintain attribution to the author(s) and the title of the work, journal citation and DOI.



Biocompatibility and degradation of the open-pored magnesium scaffolds LAE442 and La2

N Kleer-Reiter¹ , S Julmi², F Feichtner¹, A-C Waselau¹, C Klose², P Wriggers³, H J Maier² and A Meyer-Lindenberg^{1,*}

¹ Clinic of Small Animal Surgery and Reproduction, Ludwig-Maximilians-Universität, Veterinärstr. 13, München 80539, Germany

² Institut für Werkstoffkunde (Materials Science), Leibniz Universität Hannover, An der Universität 2, Garbsen 30823, Germany

³ Institute of Continuum Mechanics, Leibniz Universität Hannover, Appelstr. 11, Hannover 30167, Germany

* Author to whom any correspondence should be addressed.

E-mail: ameylin@lmu.de

Keywords: magnesium alloy, porous scaffold, μ CT, biocompatibility, osseointegration

Abstract

Porous magnesium implants are of particular interest for application as resorbable bone substitutes, due to their mechanical strength and a Young's modulus similar to bone. The objective of the present study was to compare the biocompatibility, bone and tissue ingrowth, and the degradation behaviour of scaffolds made from the magnesium alloys LAE442 ($n = 40$) and Mg-La2 ($n = 40$) *in vivo*. For this purpose, cylindrical magnesium scaffolds (diameter 4 mm, length 5 mm) with defined, interconnecting pores were produced by investment casting and coated with MgF₂. The scaffolds were inserted into the cancellous part of the greater trochanter ossis femoris of rabbits. After implantation periods of 6, 12, 24 and 36 weeks, the bone-scaffold compounds were evaluated using *ex vivo* μ CT80 images, histological examinations and energy dispersive x-ray spectroscopy analysis. The La2 scaffolds showed inhomogeneous and rapid degradation, with inferior osseointegration as compared to LAE442. For the early observation times, no bone and tissue could be observed in the pores of La2. Furthermore, the excessive amount of foreign body cells and fibrous capsule formation indicates insufficient biocompatibility of the La2 scaffolds. In contrast, the LAE442 scaffolds showed slow degradation and better osseointegration. Good vascularization, a moderate cellular response, bone and osteoid-like bone matrix at all implantation periods were observed in the pores of LAE442. In summary, porous LAE442 showed promise as a degradable scaffold for bone defect repair, based on its degradation behaviour and biocompatibility. However, further studies are needed to show it would have the necessary mechanical properties required over time for weight-bearing bone defects.

1. Introduction

Currently, the treatment of large bone defects caused by trauma, infection or tumour constitute a serious medical problem, especially when defects of critical size lack the ability to heal and impaired bone healing occurs [1, 2]. Although autografts are the gold standard for the treatment of these defects, they are associated with the problems of limited availability, additional surgery and postoperative complications [3, 4]. For this reason, there is a great demand in orthopaedic surgery for alternatives to bone grafts for bone defects. Although the use of porous ceramics and polymers as degradable bone substitutes were

some of the first implantable biomaterials, the use of degradable porous metals has become a focus of research in recent years [5–7].

Degradable bone substitutes should preferably have an osteoinductive and osteoconductive effect, as well as a good long-term biocompatibility and a degradation rate adapted to the formation of new bone [4, 5]. For successful osseointegration of scaffolds, certain structural properties such as high porosity, suitable pore size, and interconnecting pores are of particular importance [4, 8, 9]. The pores have a great influence on the immigration and ingrowth of cells and blood vessels, as well as for ensuring the nutritive supply to the ingrowing tissue. Scaffolds

with macropores between 150 and 500 μm proved to be particularly advantageous [5, 10, 11].

In addition, although it depends on the application and the stabilization technique, the bone substitutes should have similar mechanical properties to bone, both in the area of the defect and at the attachment to the surrounding bone. Current porous bone substitutes made of polymers or ceramics, such as β -tricalcium phosphate (TCP), can show good biocompatibility and osseointegration, but have low mechanical stability, so they are mainly used to fill smaller defects or are applied as coatings [12, 13]. For effective treatment of long tubular bone defects, cylindrical titanium mesh cages combined with a bone graft have been used to repair critical size bone defects [14, 15]. However, removal of the inserted titanium mesh cage is not possible after it has been surrounded by bone. Therefore, leaving the titanium mesh cages in the bone may result in stress shielding, secondary bone absorption and fracture [14, 16].

The resorbable metal magnesium and its alloys have been investigated in numerous studies for orthopaedic use due to the positive properties in context with biomedical application [13, 17, 18]. Among these positive properties are a Young's modulus similar to bone [16, 17] and a significantly higher mechanical stability compared to polymers and ceramics [13]. Furthermore, magnesium is an essential element in the body and is involved in many metabolic and enzymatic reactions [19]. However, the comparatively rapid degradation and the associated accumulation of hydrogen and corrosion products in aqueous solution are the main disadvantages of magnesium-based implants [13, 20, 21].

So far, most magnesium alloys have only been investigated as solid implants with a comparably small surface area available for corrosion. Thus, the interaction with the host tissue and the bone to scaffold interface could only be assessed to a limited extent. In contrast, open porous implants provide a larger surface area that can enhance osseointegration, but also increase the degradation rate. Therefore, these scaffolds should consist of slowly degrading magnesium alloys to ensure sufficient mechanical stability when used as a bone substitute [7]. In order to control and reduce the rapid degradation, the resistance of magnesium alloys can be tailored by selecting appropriate alloying elements. Alloys containing the elements aluminium (Al), lithium (Li), zinc and rare earths (REs) have proven to be particularly resistant [22, 23]. Screws made of the magnesium alloy MgYREZr (MAGNEZIX[®]) are already used in human medicine [24, 25].

The magnesium alloy LAE442 contains Li, Al and RE as alloying elements and has proven to be very resistant and biocompatible in many *in vitro* and *in vivo* studies in the form of intramedullary pins, cylindrical solid bodies and screw-plate systems [26–31]. The binary alloy Mg-La2 with lanthanum,

on the other hand, has only been tested *in vitro* so far and has demonstrated an improved reproducibility by using fewer alloy components [32]. In the study by Weizbauer *et al*, the alloy showed good cell compatibility and good material properties for *in vivo* evaluation [32].

In addition, many studies have shown that coatings or surface treatments of magnesium implants have a corrosion retarding effect [33, 34]. Coating with MgF_2 showed a significant reduction in magnesium degradation in the initial phase, and direct contact to the surrounding bone [35, 36]. Furthermore, better attachment and proliferation of cells could be achieved on MgF_2 -coated magnesium implants compared to uncoated ones [37]. Compared to microarc oxidation and other surface treatments, MgF_2 coating is a simple and cost-effective method suitable for industrial production [38].

The production of reproducible, porous magnesium scaffolds can be a challenge, since most manufacturing techniques, such as powder metallurgy technology, only achieve undefined pore structures [6, 7, 39, 40]. However, with the investment casting process it is possible to obtain defined interconnecting pore structures of Mg-based scaffolds with a high design flexibility [41].

Using this method, porous scaffolds made of the alloys LAE442 and Mg-La2 were produced and investigated by Julmi *et al* [42]. The *in vitro* tests showed sufficient strength of the scaffolds to withstand the forces in rabbit bone with a compression weight-bearing capacity 3.4 times (La2) and 5.6 times (LAE442) higher than the expected load [41, 42]. In the *in vivo* study by Kleer *et al* the two magnesium scaffolds LAE442 and La2 with defined interconnecting pores and MgF_2 coating were evaluated using regular radiological and *in vivo* μCT images over a period of 36 weeks [43]. In this study, slow degradation behaviour for the LAE442 scaffolds and comparatively fast degradation of the La2 scaffolds with higher gas production could already be observed.

The objective of this study was to compare the biocompatibility and the degradation mechanisms of the porous magnesium scaffolds made of the alloys LAE442 and Mg-La2 using high-resolution μCT 80 images, histological examinations and SEM/energy dispersive x-ray spectroscopy (EDX) analyses after an implantation period of up to 36 weeks.

2. Materials and methods

2.1. Scaffolds

For the present study, 80 cylindrical scaffolds (\varnothing 4 mm, length 5 mm), each with interconnecting pores (max. pore size 500 μm , porosity 41.4%), were produced from the magnesium alloys La2 ($n = 40$; 2 wt.% La) and LAE442 ($n = 40$; 4 wt.% Li, 4 wt.% Al, 2 wt.% REs) by investment casting [41]. The scaffolds were coated with MgF_2 using the conversion coating

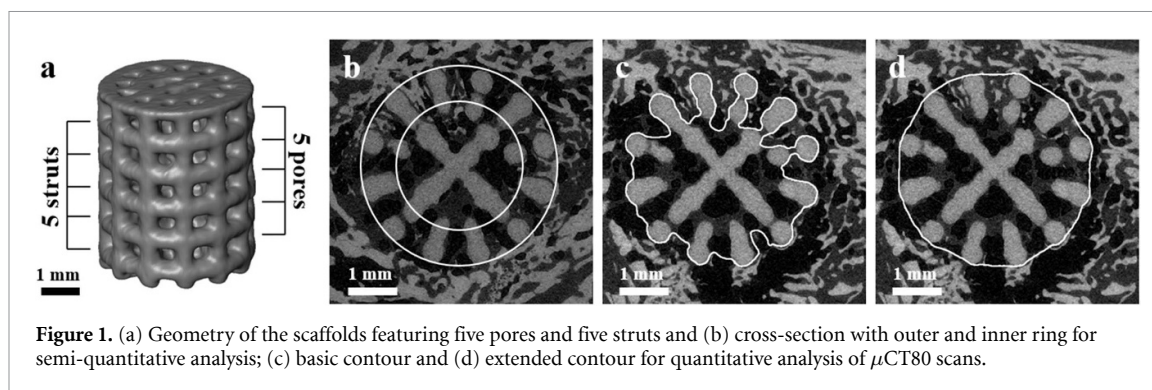


Figure 1. (a) Geometry of the scaffolds featuring five pores and five struts and (b) cross-section with outer and inner ring for semi-quantitative analysis; (c) basic contour and (d) extended contour for quantitative analysis of μ CT80 scans.

method (thickness between 450 and 1250 nm) and sterilized by gamma radiation (>25 kGy, BBF Sterilisation Service GmbH, Kern, Germany). The production process and the MgF_2 coating of the scaffolds is described in more detail in the literature [41]. A total of 40 commercially available, porous β -TCP implants (Cerasorb[®] M, Curasan AG, Kleinostheim, Germany) with the same dimensions (\varnothing 4 mm, length 5 mm, total porosity 65%) served as a control group.

2.2. Animal model

The animal experiment was approved by the government of Upper Bavaria according to the Animal Welfare Act (approval number: 55.2-1-54-2532-181-2015). A total of 60 mature female Zika rabbits (Asamhof, Kissing, Germany; \varnothing weight: 3.96 ± 0.27 kg, age: >6 months) were allocated to time groups of 6, 12, 24 and 36 weeks. For each time group, ten scaffolds of both magnesium alloys and the TCP control group were randomly inserted into the cancellous part of the trochanter major ossis femoris of the rabbits. Using a 4 mm drill, an approximately 6 mm deep hole was drilled into the cancellous part of the *greater trochanter* and the scaffolds were inserted. The exact course of the surgical procedure, as well as anaesthesia and postoperative care, are described elsewhere [43]. After the respective implantation periods, the animals were sedated with ketamine (15 mg kg^{-1} , Anesektin[®], Albrecht GmbH, Aulendorf, Germany) and medetomidine (0.25 mg kg^{-1} , Dorbene vet[®], Zoetis Deutschland GmbH, Berlin, Germany), and euthanized by intravenous application of pentobarbital (182.3 mg kg^{-1} , Narkodorm[®], CP-Pharma GmbH, Burgdorf, Germany) for the *ex vivo* examinations.

2.3. *Ex vivo* μ CT

Both femora were explanted, and all soft tissue was removed to harvest the implantation sites with a diamond band saw (Cut-grinder, patho-service GmbH, Oststeinbek, Germany). For the following investigations, the bone-scaffold compounds were fixed in a 4% formaldehyde solution for at least 14 days and positioned upright in plastic tubes fixed with foam sponges. Subsequently, *ex vivo* μ CT scans of

the bone-scaffold compounds were performed with a μ CT80 (Scanco Medical AG, Brüttisellen, Switzerland). The scan settings were: 600 ms, 70 kVp and 114 μ A with a resolution of 10 μ m. The scaffolds were manually contoured in the original scans and reoriented (Software μ CT Evaluation Program V6.6, Scanco Medical, Zurich, Switzerland) to improve the comparability as the cross-sections allowed better assessment of the scaffolds with their immediate surroundings. In order to determine the degradation of the magnesium scaffolds, scans were performed before implantation with the same scan settings and compared with the *ex vivo* scans.

2.3.1. Semi-quantitative analysis

A semi-quantitative scoring system modified according to Lalk *et al* was used to evaluate the μ CT80 images of all scaffolds [44]. The parameters scaffold degradation and scaffold shape, as well as the parameters gas within and in the direct surroundings of the scaffolds were evaluated. In addition, the structure of the surrounding cancellous bone was assessed in two areas of the scaffolds (upper and lower half of the scaffold). The integration of scaffold into bone (bone-to-scaffold contact) was evaluated on ten cross-sections (five pore and five strut levels each; cf figure 1(a)). Based on these cross-sections, the bone within the scaffolds was evaluated in an outer and an inner ring (figure 1(b)). For the TCP control group, the parameters degradation and scaffold shape were not examined due to different material properties. Score values ranged from 0 for physiological/original to 4 for clearly altered (table 1).

2.3.2. Quantitative analysis

A threshold (LAE442 160, La2 186, TCP 360) was determined for each material group and applied for the subsequent evaluations. In order to calculate the volume, density and surface area of the scaffolds after the respective implantation period of 6, 12, 24 or 36 weeks, the residual scaffolds in the reoriented scans were manually contoured by excluding the ingrown bone (basic contour; figure 1(c)). This analysis was also performed for the magnesium scaffolds before implantation to obtain the baseline values.

Table 1. Scoring system for semi-quantitative μ CT80 evaluation, modified according to Lalk *et al* [36].

Parameters	Score 0	Score 1	Score 2	Score 3	Score 4
Degradation	Not observed	Thin degradation layer	Clear degradation layer	>50% of scaffold degraded	Complete degradation
Shape of scaffold	Original	Slight changes on surface	Small portions detached	Large scaffold parts detached, > 50% altered	Complete loss of shape
Gas within/directly around scaffold	Not observed	Diffuse and few small bubbles	>25% pores or surface filled/covered	>50% pores or surface filled/covered	Pores/surface completely filled/covered
Structure of cancellous bone in vicinity	Physiologically wide-meshed	Thick (>100 μ m) and thin (<100 μ m) trabeculae	Narrow-meshed (on average 50 μ m) with occasional thick (>100 μ m) trabeculae	Small bone particles	No bone
Integration of scaffold into bone	Broad contact area to adjacent cancellous bone through many trabeculae, no/only fractional gap	Contact to adjacent cancellous bone through several trabeculae, sporadic gaps	Contact to adjacent cancellous bone through few trabeculae, clear gaps	One contact to adjacent cancellous bone, manifest gaps	No contact to adjacent cancellous bone, manifest gap
Bone within scaffold outer/inner ring	>10% of pores with bone	6%–10% of pores with bone	2%–5% of pores with bone	1% of pores with bone	No bone

In order to determine the amount of bone inside the scaffolds, an extended contour was created based on the exact scaffold rims (figure 1(d)). Therefore, the difference between the extended and the basic contour was defined as ingrown bone.

A total of seven scaffolds per material and time group were quantitatively investigated. The analyses were performed using μ CT80 scans if scaffold material could be detected and contoured. Otherwise, the scans were assessed descriptively.

2.4. Histological examination

The bone-scaffold compounds were removed from the 4% buffered formaldehyde solution and were dehydrated in a series of increasingly concentrated alcohol solutions, ending in 100%. Subsequently, xylene served as the intermedium before the samples were embedded in a plastic resin based on methyl methacrylate (Technovit® 9100, Heraeus Kulzer, Wehrheim, Germany). Using the cutting and grinding technique according to Donath, cross-sections of 70 μ m thickness were produced [45]. A central cross-section (level with pores not struts) of each bone-scaffold compound was then stained with toluidine blue O (Waldeck, Münster, Germany) [46]. The histological examinations were performed using a Zeiss Axio Imager 2 microscope (Carl Zeiss Microscopy GmbH, Jena, Germany) and Zeiss ZEN2 software (Carl Zeiss Microscopy, Jena, Germany). The samples were assessed semi-quantitatively using a scoring system, whereby score values

between 0 and 3 were assigned for all parameters (table 2).

At 25 \times magnification, a circle with a 4 mm diameter was placed around the scaffolds and the amount of scaffold material (total/cracked), bone, non-mineralized bone matrix, granulation tissue and gas were examined (figure 2). Furthermore, the parameters resorption of bone and fibrous capsule formation in the immediate vicinity of the scaffolds were assessed. For the evaluation of gas bubbles, the presence of thin fibrocyte borders was investigated to distinguish between bubbles formed *in vivo* by degradation and those formed by the preparation process.

Blood vessels and cells (fibrocytes, macrophages, foreign body cells (FBCs), neutrophil granulocytes and lymphocytes) were examined at 100 \times magnification in four areas: within a central, medial and peripheral ring in the scaffold, and direct scaffold vicinity (figure 2).

2.5. SEM/EDX

The *in vitro* and *ex vivo* degradation behaviour of the two scaffolds LAE442 and La2 was already comparatively investigated using SEM and EDX analysis in an earlier study [2]. Based on these results and the histological results from the present study, selected SEM and EDX analyses were performed with a SUPRA 55 VP (Carl Zeiss AG, Oberkochen, Germany) to investigate areas of special interest (degradation layer, MgF₂ coating, bone-to-scaffold contact, cell clusters). An acceleration voltage of 15 kV and a working distance

Table 2. Scoring system for the histological evaluation of the bone-scaffold compound cross-sections.

Parameters	Score 0	Score 1	Score 2	Score 3
Scaffold material	0%	1%–25%	26%–50%	>50%
Cracks				
Gas within/adjacent				
Bone resorption				
Bone	0%	1%–10%	11%–25%	>25%
Non-mineralized bone matrix				
Granulation tissue				
Fibrous capsule	None	Mild	Moderate	Severe
Fibrous cells (tissue)	None	Few	Moderate	Many
Vascularization (blood vessels)				
Macrophages	None	Few	Moderate	Many
FBCs				
Lymphocytes				
Neutrophil granulocytes				

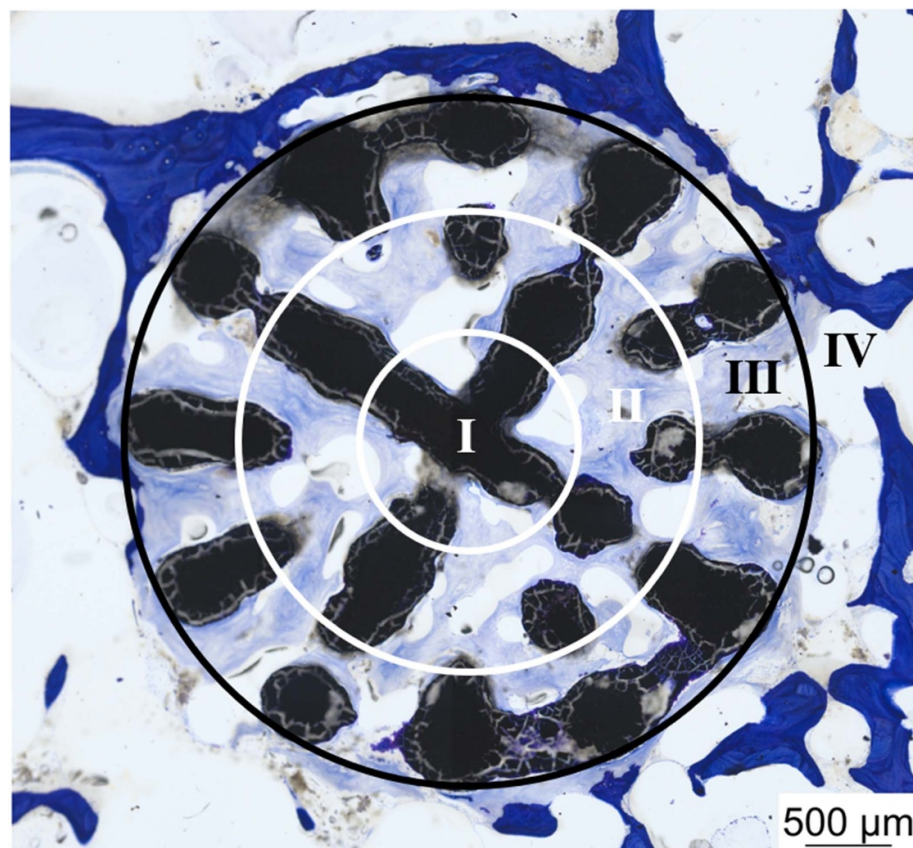


Figure 2. Histological image of scaffold cross-section; evaluation at 25× magnification, subdivided in two areas: inside and outside black circle (4 mm); evaluation at 100× magnification, subdivided in four areas: central ring (I), medial ring (II) and peripheral ring (III), and direct scaffold vicinity (IV).

of 20–25 mm for the overview images and 7.8–9.8 mm for the close-up images were used. Carbon and oxygen were excluded, as it is difficult to quantify their amount by EDX analysis.

2.6. Statistics

The data were statistically evaluated using SPSS Statistics 25.0. Since the data were not normally

distributed, Kruskal–Wallis tests were used for the evaluation and a pairwise comparison was performed with subsequent single-functional ANOVA. Subsequently, adjustments were made using the Bonferroni correction. Quantitative data on the degradation of the magnesium scaffolds were investigated using the Mann–Whitney U-test. In all analyses, a value of $p < 0.05$ was considered significant.

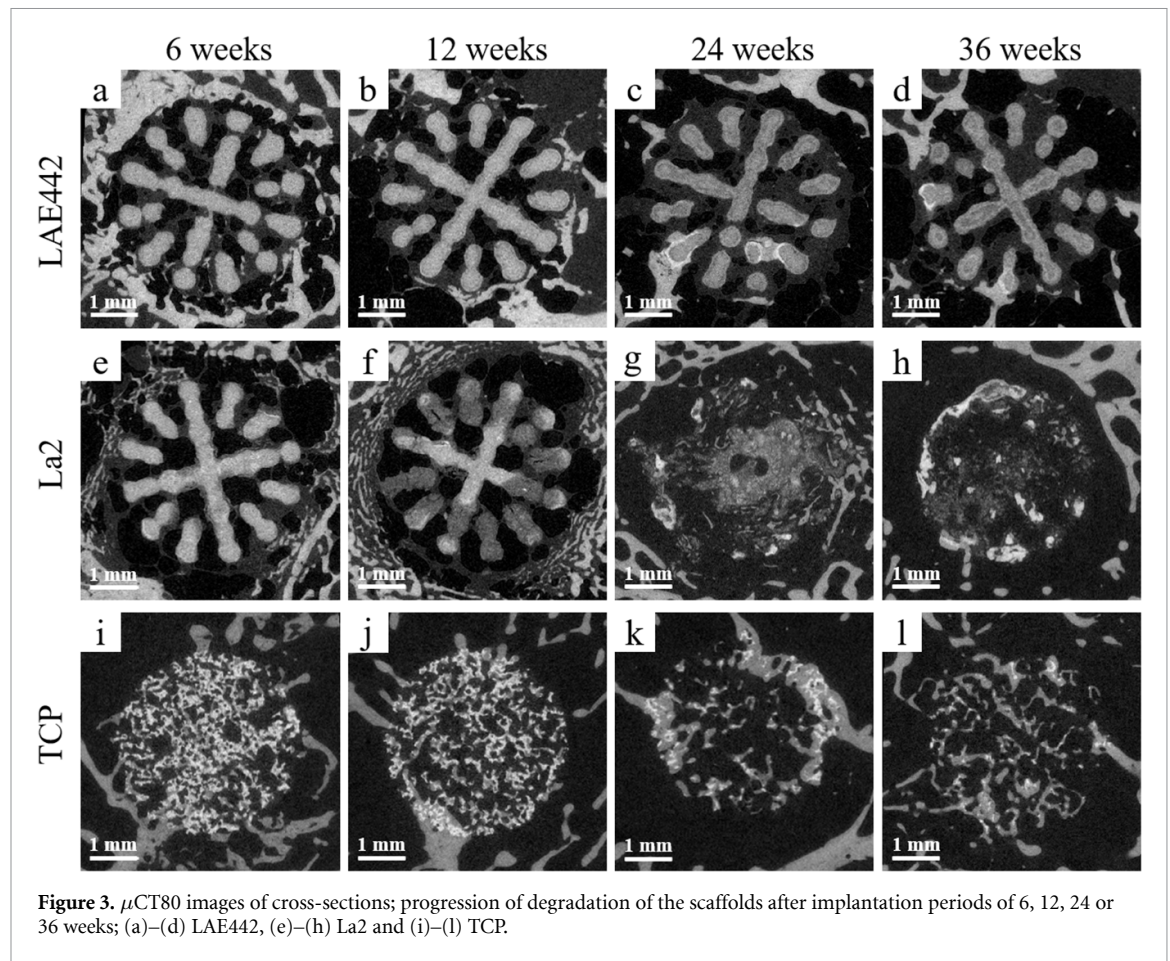


Figure 3. μ CT80 images of cross-sections; progression of degradation of the scaffolds after implantation periods of 6, 12, 24 or 36 weeks; (a)–(d) LAE442, (e)–(h) La2 and (i)–(l) TCP.

3. Results

3.1. *Ex vivo* μ CT

3.1.1. Semi-quantitative μ CT80 evaluations

Using μ CT80 images, the exact degradation behaviour of the scaffolds as well as the ingrowth of bone into the scaffolds were assessed (figure 3).

The LAE442 scaffolds showed an overall very slow and homogeneous degradation. After 6 and 12 weeks, only a thin degradation layer (score 1) was detected at the edge of the scaffolds. The scaffold shape remained unchanged (score 1) after 6 weeks and only slight surface changes (score 1) occurred after 12 weeks of implantation. After 24 and 36 weeks, all LAE442 (with one exception, week 24, score 1) showed a clearly recognizable degradation layer with small, detached parts of the scaffolds (score 2). Bright inhomogeneous areas could be observed after 6 weeks on the LAE442 scaffolds (figure 4(a)), which increased strongly in size and number until week 36. In contrast, the La2 scaffolds showed rapid and inhomogeneous degradation. After 6 weeks, a clear degradation layer (score 2) was visible with detachment of increased small and occasionally large scaffold particles (score 2 and 3). A single La2 scaffold was already completely degraded (score 4). More than 50% of the La2 scaffolds were degraded after 12 weeks (score 3; with one exception, score 2), and large portions of the scaffolds

were separated (score 3). From 24 weeks onwards, all La2 scaffolds (with one exception, week 24, score 3) were completely degraded and the shape of the scaffold was no longer recognizable (score 4). Overall, the La2 scaffolds showed significantly faster degradation and loss of shape in all week groups compared to the LAE442 scaffolds ($p < 0.001$).

In contrast to the TCP control group, accumulation of gas could be detected in the scaffolds made from the two magnesium alloys. The highest accumulation of gas was found in La2 after 12 weeks. More than 50% of the internal space (pores) was filled with gas and more than 50% of the direct surface was surrounded by gas. Subsequently, at week 24 only small amounts of gas were observed and at week 36 no gas was found. In contrast, LAE442 showed a relatively constant gas accumulation directly around the scaffolds, which covered at least 25% and sometimes more than 50% of the surface, over all observation times. Within the LAE442 scaffolds, more than 25% and up to 50% of the interstices were filled at the early implantation points, and mainly small gas bubbles were observed at the later implantation points.

In all time groups, bone in the vicinity of the LAE442 scaffolds mainly showed a mixture of thick and thin trabeculae, which was more pronounced in the upper half of the scaffolds near the drill hole (figure 5(a)). In the lower part near the medullary

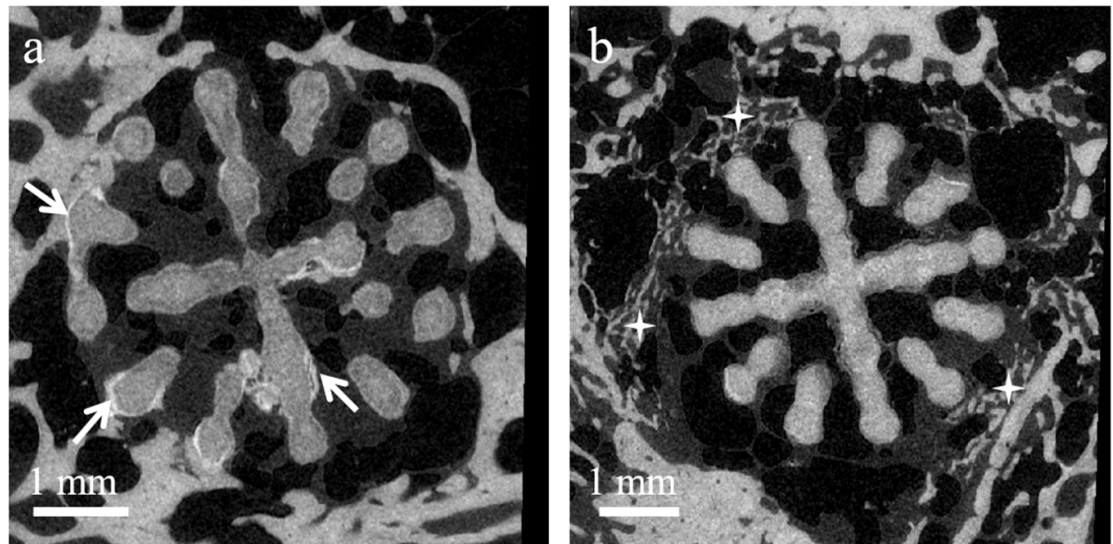


Figure 4. μ CT80 images: (a) LAE442 scaffold 36 weeks after implantation, arrow: bright appearing deposits (Ca/P) on scaffold surface; (b) La2 scaffold 6 weeks after implantation, star: narrow-meshed bone trabeculae.

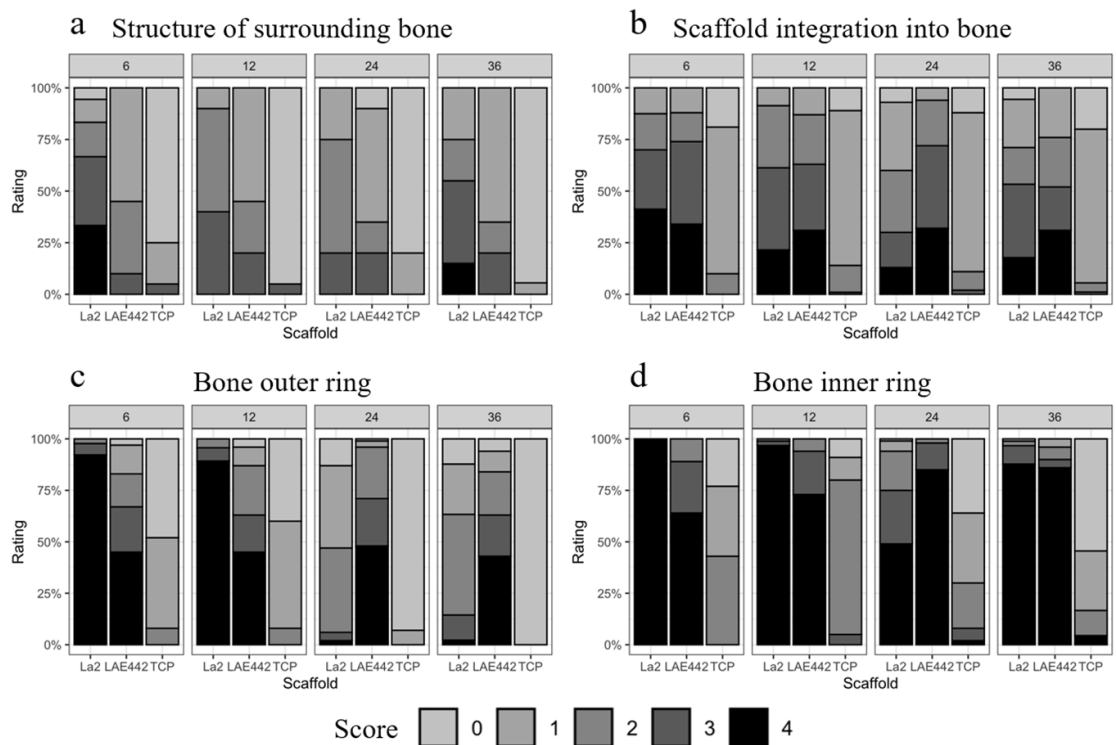


Figure 5. Semi-quantitative analysis of the μ CT80 scans showing the parameters after the implantation periods of 6, 12, 24 and 36 weeks: (a) structure of surrounding bone, (b) scaffold integration into bone, (c) bone in outer ring and (d) bone in inner ring; score values ranged from 0 for physiological/original to 4 for clearly altered (table 1).

canal, thin, narrow-meshed bone trabeculae and occasionally only small bone particles could be observed around the LAE442 scaffolds. The structure of the cancellous bone around the La2 scaffolds was very inhomogeneous. In all week groups, often only very small bone fragments and in some cases a mixture of mostly thin and thick trabeculae occurred (figure 5(a)). In some cases of the 6— and 36—weeks group, no bone was found in the vicinity

of the La2 scaffolds. An increased occurrence of thin, narrow-meshed bone trabeculae was observed after 12 and 24 weeks (figure 5(b)). The TCP control group showed mainly a widely cross-linked, spongy bone and occasionally a mixture of thick and thin trabeculae in all time groups (figure 5(a)).

For the parameter ‘integration of scaffold into bone’, LAE442 showed an average of one direct contact per cross-section at all observation times, with

a slight increase after 36 weeks. Although several bone trabeculae and in some cases large bone bridges occurred around most of the LAE442 scaffolds, these did not have direct contact to the scaffold but were separated by narrow gaps. However, isolated LAE442 scaffold areas also showed larger distances to the surrounding cancellous bone (figure 5(b)). The La2 scaffolds also showed on average one direct contact per cross-section after 6 and 12 weeks. Compared to LAE442, the distances between the surrounding cancellous bone and the La2 scaffolds were considerably larger. In the La2 week group 24 and 36, increased contact between a few bone trabeculae and the degraded scaffold residues could be detected (figure 5(b)). The TCP implants showed close contact to the cancellous bone through several bone trabeculae punctuated with isolated gaps at all observation times (figure 5(b)).

For the parameter 'bone in the scaffold', about 2%–5% bone was observed in the LAE442 scaffolds after 6 weeks in 5/10 scaffolds in the outer ring and about 1% bone in 3/10 scaffolds in the inner ring (figures 5(c) and (d)). In the remaining LAE442 scaffolds, no bone could be found after 6 weeks. At the subsequent implantation points, bone ingrowth in the pores became increasingly inhomogeneous, with the majority showing no bone or isolated small bone fragments in the outer area. However, in a few samples up to 10% bone within the pores of the LAE442 scaffolds could be observed. In comparison, no bone within the pores could be detected after 6 and 12 weeks in the La2 scaffolds. After 24 and 36 weeks, about 2%–5% bone in the outer area between the degraded scaffold residues could be observed. In the inner area, small bone trabeculae occurred only in single cases after 24 weeks of implantation. After 36 weeks, no bone was visible in the centre (figures 5(c) and (d)). The TCP implants showed the best values within the pores after 6 and 12 weeks, with an average of about 6%–10% bone in the outer ring and 2%–5% in the inner ring. After 24 and 36 weeks, TCP had over 10% bone in the outer ring and about 6%–10% in the inner ring (figures 5(c) and (d)). Within the TCP implants, significantly more bone was found at all observation times than in the magnesium scaffolds ($p < 0.001$). LAE442 showed significantly more bone in the outer ring after 6 and 12 weeks ($p < 0.001$) in comparison to La2. At the original implantation site of La2, significantly more bone was observed after 24 and 36 weeks ($p < 0.001$) as compared to LAE442.

3.1.2. Quantitative μ CT80 evaluation

Due to the almost complete degradation of the La2 scaffolds after 24 and 36 weeks, the quantitative evaluations for these scaffolds could only be performed for the observation times 6 and 12 weeks.

Continuous and slow degradation of the scaffolds was observed in the LAE442 group, which was

accompanied by a volume loss of 7.46% (2.7 mm^3) by week 36. In comparison, a volume loss of 62.72% (22 mm^3) with inhomogeneous degradation behaviour could already be observed in the La2 scaffolds after 12 weeks. The LAE442 scaffolds showed significantly more volume ($p = 0.001$) as compared to La2 at week 6 and 12. In terms of density, the LAE442 scaffolds showed a slight increase at all observation times as compared to their original density. A similar increase in density was observed in the La2 scaffolds after 6 and 12 weeks (figures 6(a) and (b)).

Analysis of the ingrown bone of LAE442 after 6 weeks revealed an average of 0.55 mm^3 bone-like fractions in the pores of the scaffolds. After 12 and 24 weeks, the proportion of bone in the pores decreased, and at 36 weeks an average of 0.36 mm^3 bone-like fractions within the pores could be observed (figure 6(c)). In the La2 scaffold, bone-like fractions averaging 0.05 mm^3 after 6 weeks and small bone fragments averaging 0.19 mm^3 after 12 weeks were observed in the outermost region of the already severely degraded scaffold sections (figure 6(c)). In the TCP control group, many small bone trabeculae between the implant residues (average 24.29 mm^3 bone) could be detected after 6 weeks. At all subsequent observation times, fewer but thicker bone trabeculae (average 18.64 mm^3 bone) occurred, which enclosed the remaining implant parts.

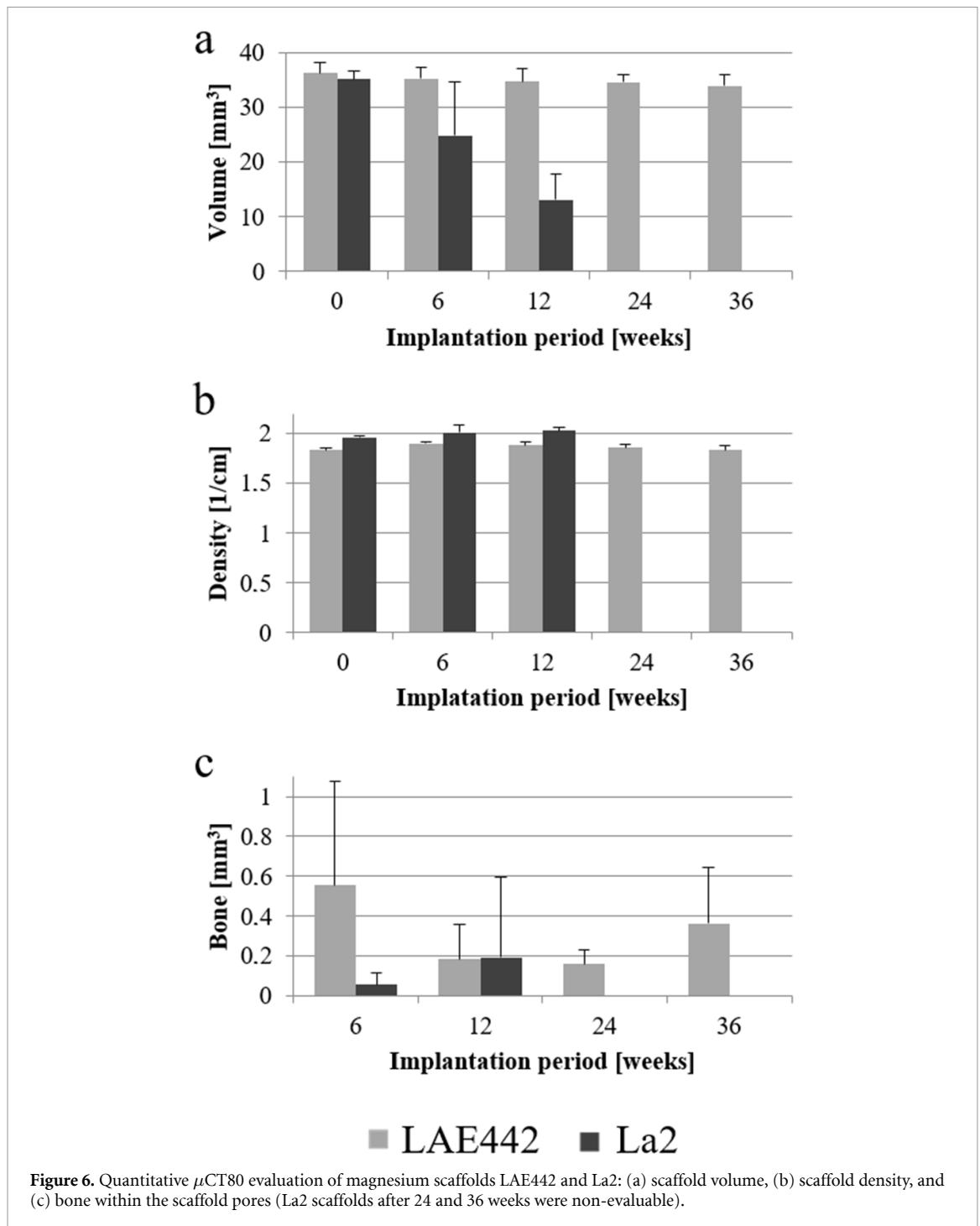
3.2. Histological examination

In the evaluation of the central cross-section, the La2 scaffolds showed rapid degradation with significantly less scaffold material ($p < 0.001$) after 24 and 36 weeks as compared to LAE442 (figures 7(a)–(h)). In contrast, the LAE442 scaffolds remained relatively constant with respect to the amount of material and only showed an increasing amount of 'cracked' degradation layer until week 36.

Until week 12, LAE442 showed more bone within the scaffolds in the central cross-section as compared to La2. After 24 weeks, more bone in the form of thin bone trabeculae between the La2 residues was observed as compared to LAE442. These bone trabeculae decreased again after 36 weeks in the area of the original scaffold localization of La2 (figure 8(b)).

LAE442 in particular showed an increasing amount of poorly mineralized, osteoid-like bone matrix within the scaffold pores of more than 25% by week 24, with an increasing number of empty osteocyte lacunae over time. Between the remains of the La2 scaffolds, poorly mineralized bone matrix was also observed after 24 and 36 weeks (figure 8(c)).

After 6 and 12 weeks, granulation tissue was rarely present in La2 and only in the peripheral area of these scaffolds. The La2 scaffolds showed a strong accumulation of gas within the scaffolds. From week 24 onwards, a small accumulation of gas and more granulation tissue between the scaffold residues of La2 were observed. No gas could be detected in La2 after



36 weeks (figures 8(a) and (d)). Within the LAE442 scaffolds, the low to moderate gas accumulation as well as the amount of granulation tissue (<10%), which was also found in the scaffold centre, decreased slightly over the observation period (figures 8(a) and (d)). After 24 and 36 weeks, LAE442 showed significantly less granulation tissue ($p < 0.001$) and after 36 weeks significantly more gas ($p < 0.001$) compared to the La2 scaffolds. In the TCP control group, no gas in and around the scaffolds and more than 25% granulation tissue within the implants could be observed at all time groups (figures 8(a) and (d)).

After 6 and 12 weeks, half of the La2 cross-sections were surrounded by up to 50% by gas and in the other half over 50% of the implant surface was surrounded by gas. In two cases, after 24 weeks up to 25% of the remaining scaffold material was still covered by gas and after 36 weeks no gas was found around the La2 residues. In the LAE442 scaffolds, the gas accumulation in the direct vicinity of the scaffold remained relatively constant at all observation times between 25% and 50% (score 2) and over 50% (score 3) with a maximum after 24 weeks.

Direct bone-to-scaffold contact was observed only in single LAE442 cross-sections at several sites.

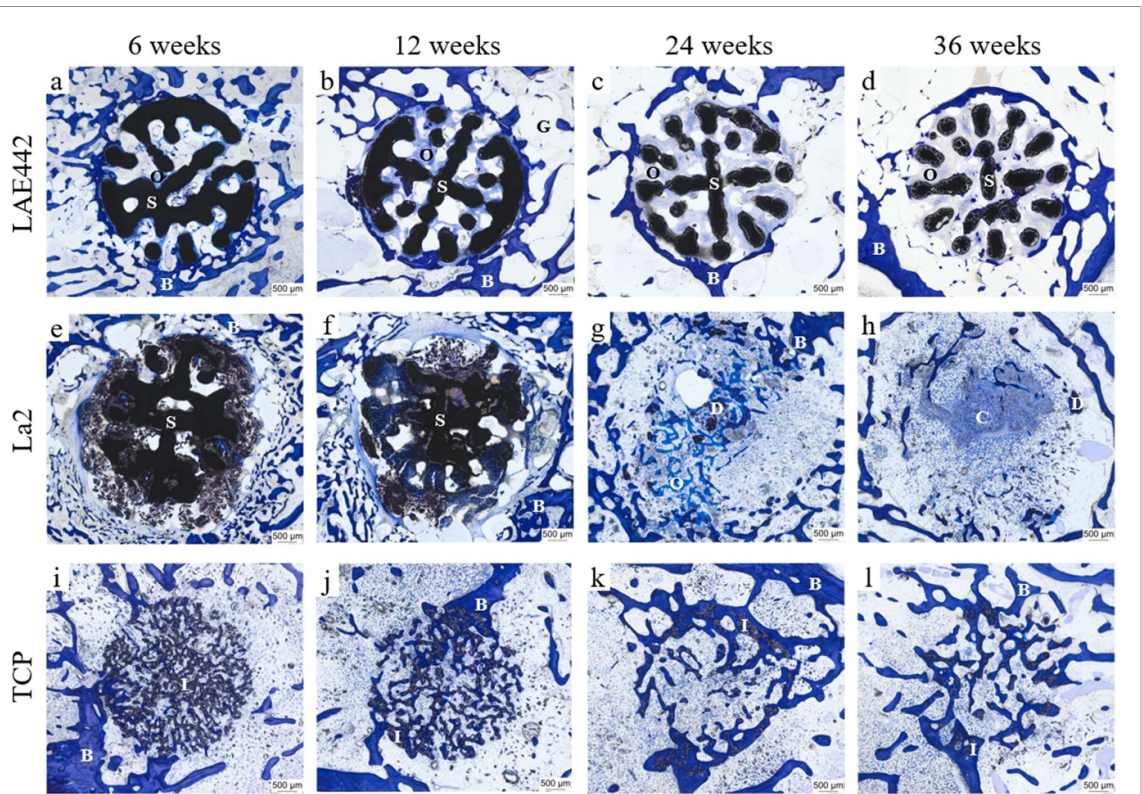


Figure 7. Histological cross-sections of LAE442, La2 and TCP, toluidine blue: (a)–(d) LAE442, (e)–(h) La2 and (i)–(l) TCP; B = bone, G = gas, O = osteoid-like non-mineralized bone matrix, S = scaffold material (magnesium), I = implant material (TCP), FC = fibrous capsule, D = debris, C = cell cluster.

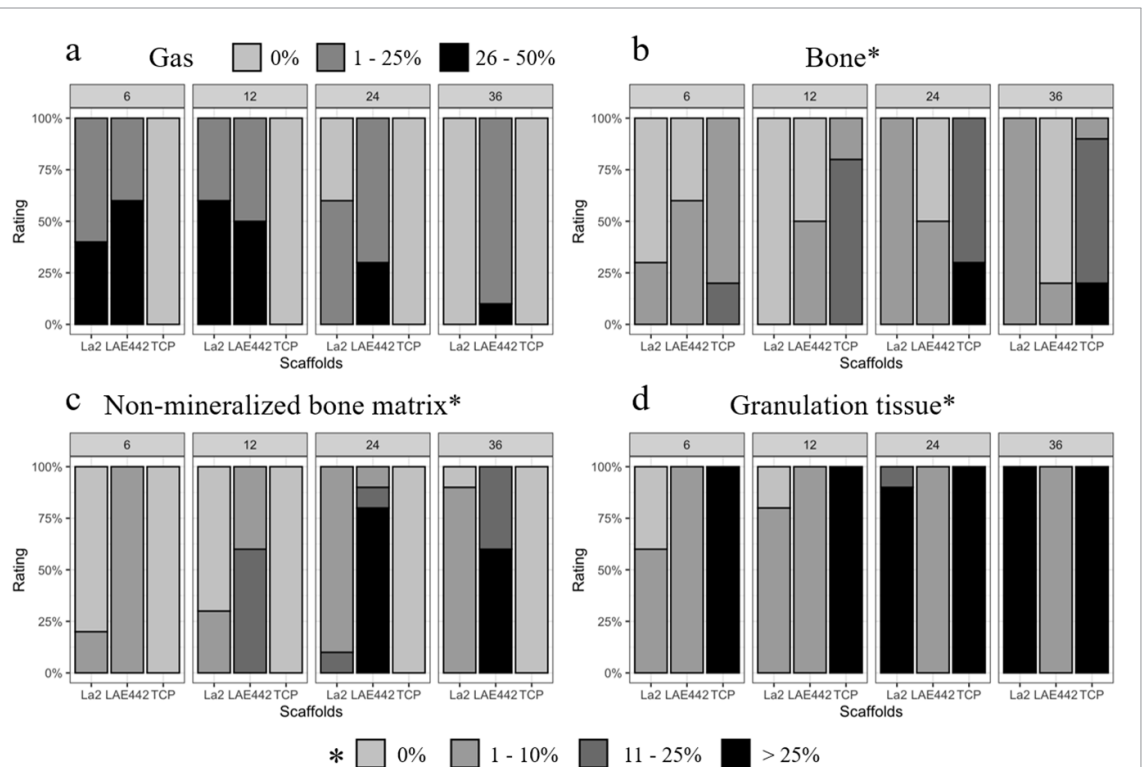


Figure 8. Results of the histological evaluation (25× magnification) within the scaffold (4 mm diameter circle): (a) gas, (b) bone, (c) non-mineralized bone matrix, and (d) granulation tissue.

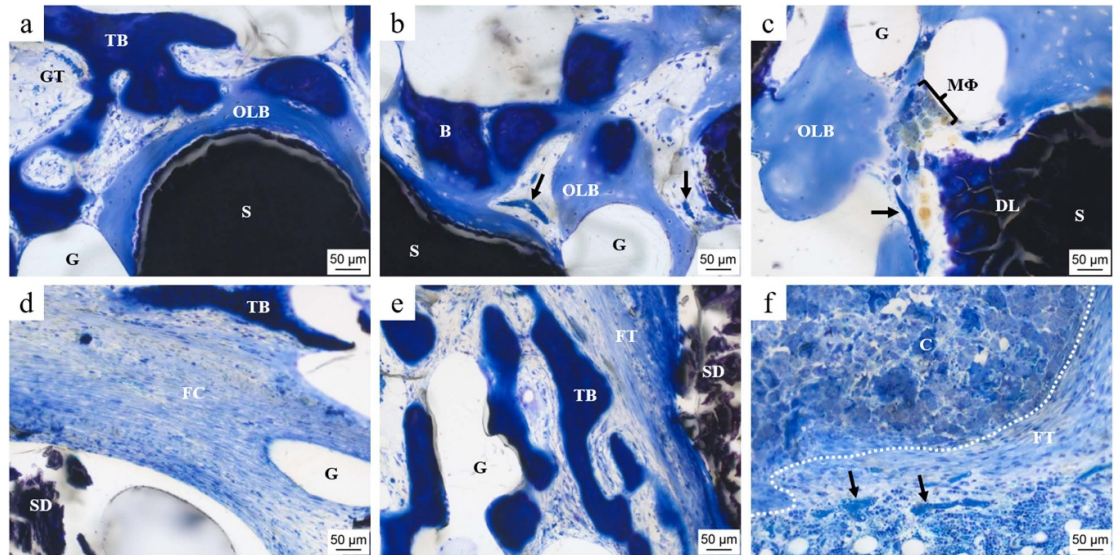


Figure 9. Histological images, toluidine blue: (a), (b) LAE442 after 6 weeks, (c) LAE442 after 24 weeks, (d), (e) La2 after 12 weeks and (f) La2 after 36 weeks; S = scaffold, SD = scaffold debris, DL = degradation layer with cracks, B = bone, TB = trabecular bone, G = gas, GT = granulation tissue, OLB = osteoid-like bone matrix, FC = fibrous capsule, FT = fibrous tissue, C = cell cluster (macrophages and FBCs; marked with white dotted line), M Φ = macrophages (marked with black brace), black arrows = blood vessels.

In the majority of the LAE442 scaffolds, a connection between the scaffold material and the surrounding bone could be demonstrated via a poorly mineralized bone matrix (figure 9(a)). The proportion of the poorly mineralized bone substance surrounding the scaffold surface increased significantly over time. In La2, direct contact between the scaffold and the surrounding bone by isolated bone trabeculae was observed in individual cases after 6 and 12 weeks. Otherwise, strong resorption of the surrounding cancellous bone was visible. After 24 and 36 weeks, the remaining La2 scaffold residues were directly enclosed by bone.

A fibrous capsule formation around the scaffolds was observed in La2 in varying degrees after 6 and 12 weeks (figures 9(d) and 10(a)). In addition, a strong network of thin trabeculae formed behind and between the fibrous tissue at some distance from the scaffolds (figure 9(e)). In comparison, only a moderate number of fibrocytes in the granulation tissue could be detected in LAE442 (figure 10(a)).

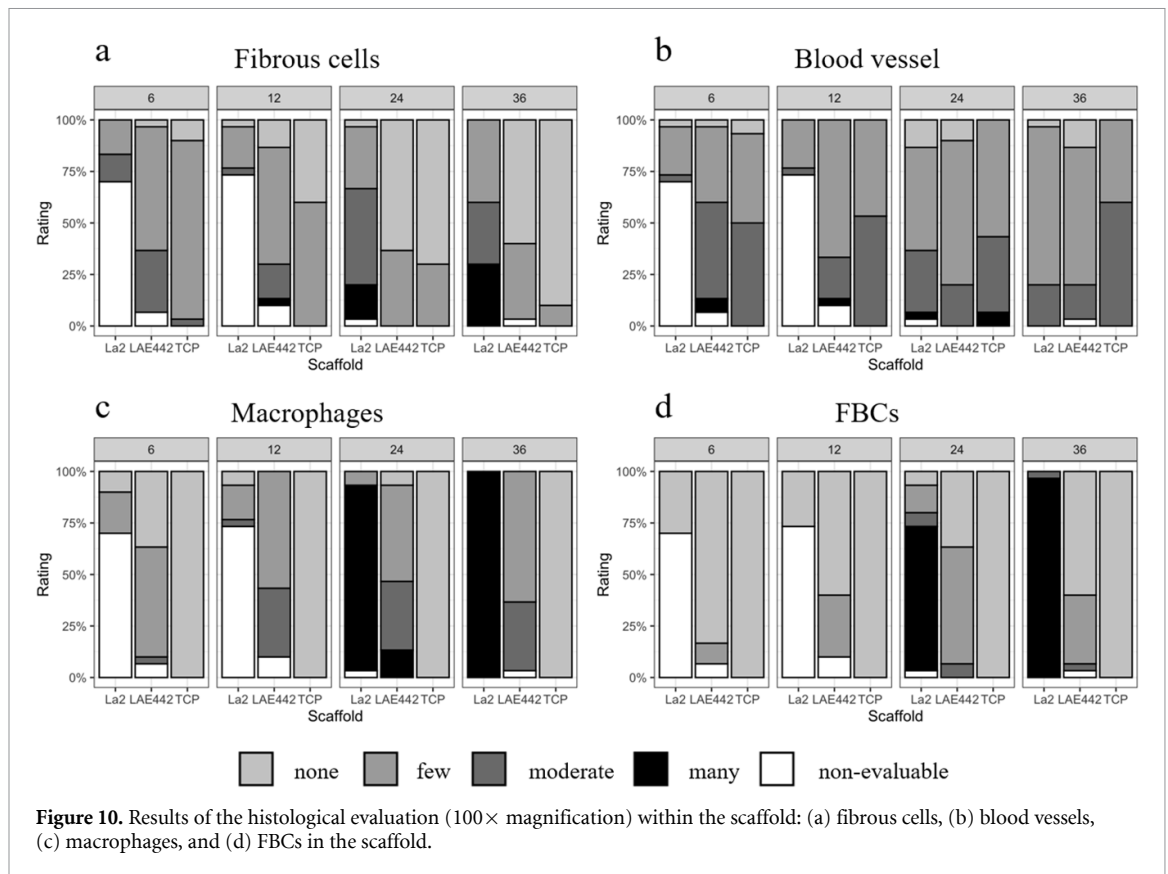
In the LAE442 scaffolds, a moderate number of blood vessels was found after 6 and 12 weeks (figures 9(b) and 10(b)), with slightly fewer blood vessels in the centre of the scaffolds as compared to the peripheral area. Subsequently, after 24 and 36 weeks, the number of blood vessels decreased and only a few were present within the scaffolds (figures 9(c) and 10(b)). In the La2 scaffolds, no or only isolated blood vessels could be observed in the marginal area of the scaffolds after 6 and 12 weeks of implantation. After 24 and 36 weeks, few blood vessels appeared between the La2 residues. TCP showed a moderate number of

blood vessels within the implant residues in all time groups (figure 10(b)).

LAE442 demonstrated an overall increasing but moderate number of macrophages and a few FBCs in and around the scaffolds over the entire observation period. In La2, no macrophages and FBCs were observed in the central or middle area of the scaffolds after 6 and 12 weeks. However, an increasing number of macrophages and FBCs occurred in the immediate vicinity of the La2 scaffolds (figures 10(c) and (d)). From week 24 onwards, a strong accumulation of macrophages and FBCs was observed in the centre of the original scaffold localization (figure 9(f)). The TCP control group showed no foreign body reaction (macrophages and FBCs) and had sporadic neutrophil granulocytes. Overall, no signs of an inflammatory reaction could be observed in any material group.

3.3. SEM/EDX

The SEM images of LAE442 revealed a darker degradation layer with increasing extent over time with an accumulation of calcium and phosphorus [2]. In some places the degradation layer had a double-layered structure with a bright outer and a darker underlying part (figures 11(a) and (b)). Comparing these two layers, the darker layer had a higher magnesium content and the brighter layer had a higher calcium and phosphorus content (table 3). On the scaffold surface of LAE442, fluorine, a component of the MgF₂ coating, could be detected to varying extents depending on localization and implantation period. A general decrease could be observed to 0.8 wt.% fluorine after 36 weeks. Furthermore,



the contact between the scaffold material of LAE442 and the surrounding bone was often observed via an intermediate matrix with calcium and phosphorus as the main components (table 3). This scaffold-matrix-bone connection was increasingly observed in the implantation periods of 24 and 36 weeks (figures 11(c) and (d)).

In the La2 scaffolds, the scaffold material and the strongly increasing degradation layer could be identified in the SEM images only until 12 weeks after implantation. Thereby fluorine was detected on the scaffold surface with 22.8 wt.% after 6 weeks and 1.6 wt.% after 12 weeks. From week 24 on, small degraded scaffold particles, as well as bone and clusters of small, roundish structures (identified on the histological sections as cell clusters of macrophages and FBCs) could be observed in the original implantation area using SEM images (figures 11(e) and (f)). Within the described cell clusters, the EDX analysis of a La2 cross-section after 36 weeks showed a strong accumulation of lanthanum of up to 67.3 wt.% (table 3).

4. Discussion

The objective of the present study was to compare the biocompatibility, the ingrowth of the surrounding tissue and the degradation behaviour of the magnesium scaffolds La2 and LAE442 with defined interconnecting pores *in vivo*. Commercially available porous β -TCP implants of the same dimensions served

as a control group. So far, the alloy LAE442 has been investigated in many *in vivo* studies only as solid implants, such as intramedullary pins or screws [27–29]. The binary alloy Mg-La2 exhibited good properties *in vitro*, allowing the investigation of this alloy *in vivo* [32]. Previous investigations focused mainly on magnesium scaffolds with a random and irregular pore distribution [7, 33, 40, 44, 47]. In order to increase the reproducibility and stability of the implants, magnesium scaffolds with defined pore structures were developed for this study. *In vitro* investigations by Julmi *et al* showed sufficient stability of the open-pored magnesium scaffolds LAE442 and La2 to withstand the forces occurring in the rabbit bone [41]. In the study by Kleer *et al*, these two alloys LAE442 and Mg-La2 were examined *in vivo* in the form of open-pored magnesium scaffolds in the rabbit model by means of clinical, radiological and μ CT analyses, and LAE442 in particular showed a slow and homogenous degradation [43]. In the present *in vivo* study, each bone-scaffold compound was examined in more detail after the respective observation time of 6, 12, 24 or 36 weeks using high-resolution μ CT80 scans. In addition, histological examinations were conducted to assess biocompatibility and EDX analyses were performed on cross-sections to evaluate the distribution of elements in areas of special interest.

Using *ex vivo* μ CT80 scans, the degradation of the scaffolds could be assessed in higher resolution compared to the *in vivo* μ CT images of the study by Kleer *et al* [43]. The *ex vivo* scans revealed the degradation

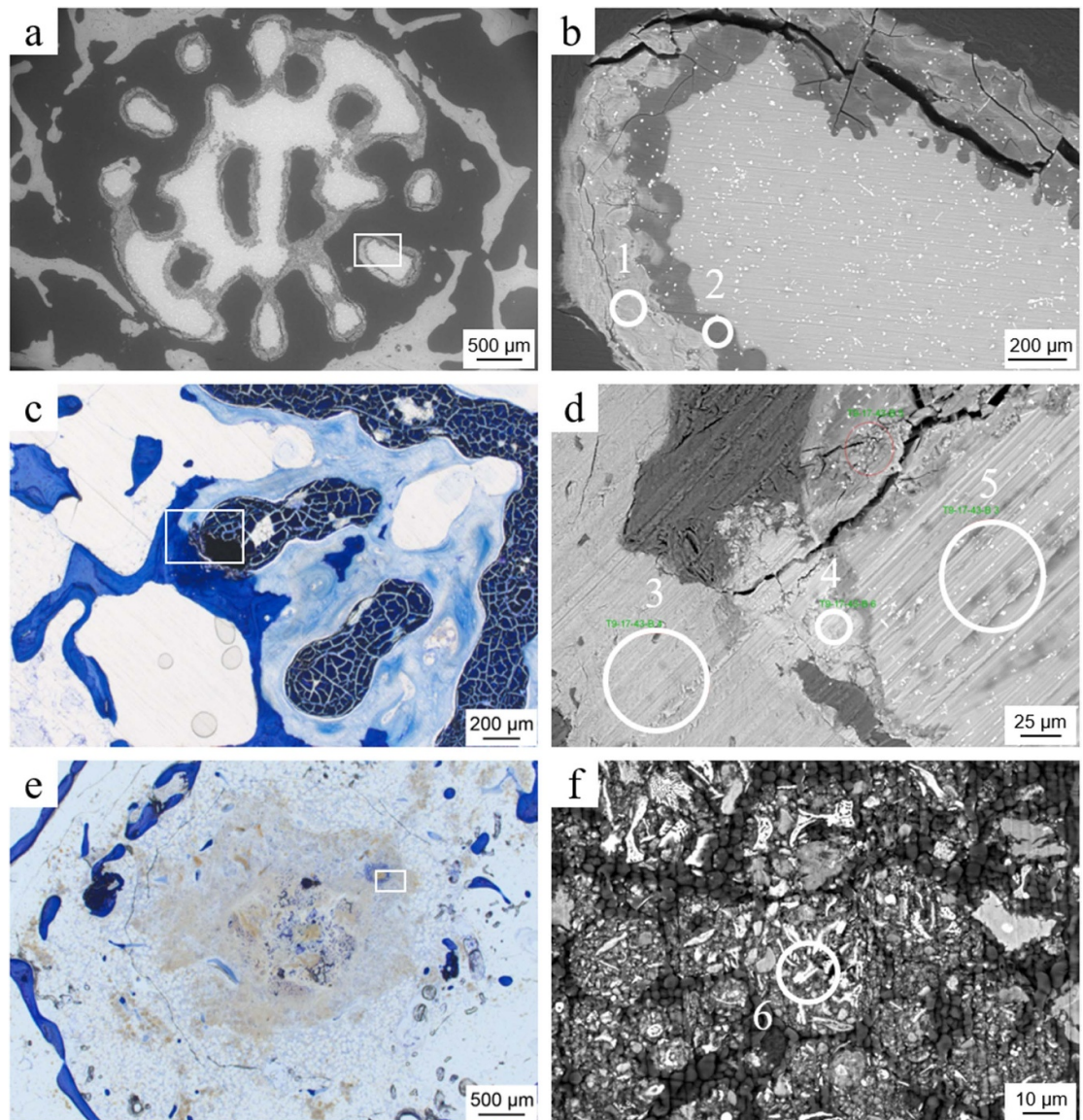


Figure 11. SEM and histological images: (a), (b) SEM images of LAE442 after 24 weeks, degradation layer, double-layered structure with bright outer (1) and darker underlying (2) part; (c) LAE442 after 36 weeks (d) magnification: intermediate matrix (4) as contact between bone (3) and scaffold (5); (e) La2 after 36 weeks: large cell clusters (macrophages and FBCs), (f) magnification: roundish structures with bright particles; positions (1–6) marked in (b), (b) and (f) indicate the locations of the EDX analyses presented in table 3.

layer and bright deposits on the scaffolds. These bright deposits were probably the accumulation of calcium and phosphorus, as verified in the EDX analyses of the LAE442 scaffolds. In the μ CT80 images of LAE442 fine gaps were often visible between the surrounding bone trabeculae and the scaffold, which could not be detected in the *in vivo* investigations by Kleer *et al* [43]. Using the histological sections these apparent gaps could be determined as an osteoid-like bone matrix. As described in other studies, this was a poorly mineralized bone matrix and therefore did not appear bone dense in the μ CT80 images [33, 48]. As a result, less frequent direct bone-to-scaffold contacts were evaluated for LAE442 in the present study compared to the study by Kleer *et al* [43]. As in the *in vivo* study [43], one direct bone-to-scaffold contact

per cross-section was observed on average for the La2 scaffolds. In most cases, one thick bone trabeculae grew from the periphery directly to the La2 scaffolds with otherwise large gaps to the surrounding cancellous bone. This observation of inhomogeneous integration also occurred in the study by Lalk *et al* on porous AX30 magnesium scaffolds with CaP-coating. Many of the scaffolds had completely lost contact with the surrounding cancellous bone and exhibited wide gaps [33].

In the μ CT80 images, isolated bone dense islands within the pores of the LAE442 scaffolds were observed, most of which had no direct contact to the scaffold material. This phenomenon of isolated bone islands was also observed by Lalk *et al* within the pores of the MgF₂-coated AX30 scaffolds. These bony

Table 3. EDX data for LAE442 and La2 scaffolds: LAE442 after 24 weeks, degradation layer, dark part (position 1) and bright part (position 2); LAE442 after 36 weeks, bone-to-scaffold contact, bone (position 3), intermediate matrix (position 4), scaffold (position 5); La2 after 36 weeks, cell clusters, within a cell (position 6); positions 1–6 are marked in figure 10.

Element	Concentration in wt.%					
	LAE442 24 weeks		LAE442 36 weeks			La2 36 weeks
	1	2	3	4	5	6
Mg	72.7	32.0	7.8	23.1	89.2	1.0
Al	12.9	4.5	0.7	2.6	3.4	1.6
La	0.2	—	—	—	0.6	67.3
Ce	1.3	2.0	—	—	1.1	—
Si	0.3	0.2	0.8	0.2	0.5	—
P	3.8	17.7	26.3	17.6	1.6	18.7
Ca	6.8	41.4	62.4	53.9	3.0	9.2
Na	1.1	2.2	1.6	2.5	—	—
S	0.1	—	0.4	—	0.6	1.1
K	—	—	—	—	—	0.2
Fe	—	—	—	—	—	1.0
Mn	0.4	—	—	—	—	—
Cl	0.4	—	—	0.2	—	—

islands were surrounded by poorly mineralized bone matrix which did not appear bone dense in μ CT80 [33]. The presence of poorly mineralized bone matrix could be confirmed in the present study using the histological sections.

In assessing the structure of the surrounding bone, TCP mainly showed a physiological wide-meshed bone structure, as also observed in the control group ‘empty drill holes’ after 12 and 24 weeks in the study by Lalk *et al* [33]. This wide-meshed bone could only be observed after 24 weeks around the AX30 MgF₂-coated scaffolds and only in half of the CaP-coated scaffolds [33]. The remaining CaP-coated scaffolds showed only a narrow-meshed bone structure at 24 weeks [33], which could also be observed within a certain range around the La2 scaffolds after 6 and 12 weeks. In comparison, the LAE442 scaffolds in the present study exhibited a better bone structure in the immediate vicinity with mostly a mixture of thin and thick trabeculae and only a few large gaps.

μ CT80 images of the bone-scaffold compounds showed, accumulation of gas within and directly around the magnesium scaffolds, but not in the TCP control group. During the degradation of magnesium, hydrogen is formed, which accumulates if it cannot be sufficiently absorbed or removed by the surrounding tissue and blood vessels [13, 20]. However, in the *in vivo* study by Kleer *et al* and in other studies, the accumulation of gas inside the bone had no clinical effects such as lameness or signs of pain on the animals [43, 49, 50].

The histological evaluation of implants is one of the most important methods for assessing their biocompatibility [51]. In the present study, as well as in many other studies [44, 52, 53], parameters such as newly formed bone and osteoid, the amount of blood vessels and fibrous tissue, as well as inflammatory reactions and foreign body reactions (particularly

evident in the presence of macrophages and FBCs) were examined.

In addition, the evaluation of the scaffold material in the present histological examination revealed ‘cracks’ in the degradation layer of the LAE442 scaffolds to an increasing extent over the implantation periods. Ullmann *et al* microscopically observed cracks on the implant surface of LAE442 pins after an implantation period of 6 months [30]. In the study by Rössig *et al*, cracks in the degradation layer of the LAE442 implants in the sheep model were visible in the histological sections after 24 weeks [54]. As early as 1900, while investigating Mg implants for vascular surgery, Payr reported a rough surface on the implants after 24 h and many furrows and cracks in the implants after three to four days up to the complete dissolution of the metal [55]. However, the ‘cracks’ in the present study could also be artefacts formed in the more unstable degradation layer during the preparation of the histological samples. In the study by Kraus *et al*, cracks in the oxide layer of Fe-based implants were attributed to dehydration during sample preparation [56]. Subsequent investigations are necessary to clarify this phenomenon and the possible impact on the stability of the scaffolds.

More bone within the scaffolds was found in LAE442 compared to La2 by week 12. Small, thin bone trabeculae were detected after 24 weeks in the original scaffold localization of La2, after only residuals of the scaffolds and hardly any gas remained. This phenomenon of regeneration of the surrounding bone was also observed in the study by Kraus *et al* after almost complete degradation of ZX50 implants and thus decreasing gas formation [57].

In the present study, an increasing amount of poorly mineralized, osteoid-like bone matrix was found over the implantation periods, especially within the pores of the LAE442 scaffolds. A few pores

of LAE442 were completely filled with this poorly mineralized bone matrix. The study by Lalk *et al* also revealed unusually wide osteoid formations of up to 220 μm in the area of porous AX30 magnesium scaffolds [33]. To a lesser extent, this was also observed in the original scaffold localization of the La2 scaffolds after 24 and 36 weeks in the form of thin, poorly mineralized trabeculae. Significantly more osteoid compared to the control group was also found in the study by Witte *et al* in the peri-implant area around the porous AZ91D scaffolds [40]. Besides other factors, the fluoride in the coating could lead to increased osteoid formation by stimulating osteoblastic activity and delay the mineralisation of new bone. This mechanism was described by Mousny *et al* after oral application of fluoride in a mouse model [48]. Furthermore, there is a controversial discussion in the literature about whether aluminium, which is a component of the LAE442 alloy, has a negative influence on mineralisation and delays this process [58–60]. The exact mechanisms of incomplete mineralization could not be conclusively clarified in this study. However, it appears to be a multifactorial process, since the osteoid-like bone matrix was present in both magnesium alloys to a different extent.

Within the pores of LAE442 scaffolds, a moderate number of blood vessels could be detected histologically in the early time groups (6 and 12 weeks), as well as within the TCP implants at all implantation times. In contrast, no blood vessels were found within the La2 scaffolds after 6 and 12 weeks and subsequently (24 and 36 weeks), as with the LAE442 scaffolds, only a few blood vessels were observed. Vascularisation in the area of the bone graft substitutes is of critical importance for osseointegration [9]. In the study by Cheng *et al*, the 400 PMg scaffolds with the larger pores in a rabbit model showed higher vascularisation compared to the smaller pore size, which could be the reason for the increased bone formation [47]. Overall, the TCP control group showed the best vascularization and osseointegration in the present study, as well as the largest amount of ingrown bone compared to both magnesium scaffolds. However, the mechanical properties such as the stability of β -TCP are not sufficient for the application in weight-bearing bone defects [12].

The presence of macrophages and FBCs, as well as the formation of granulation tissue, is considered to be a normal response to implanted degradable biomaterials [4]. In the long-term study by Angrisani *et al*, investigating intramedullary LAE442 pins in a rabbit model, the presence of macrophages and giant cells for removal of corrosion products of the LAE442 pins was assessed as good cellular compatibility [26]. Therefore, the mild to moderate presence of macrophages and FBCs in the LAE442 scaffolds is considered as a normal reaction to the biomaterial during the degradation process and indicates good biocompatibility. In comparison, no or hardly any

granulation tissue and thus no cells were detected due to gas within the pores of the La2 scaffolds after 6 and 12 weeks. Subsequently, a very strong accumulation of macrophages and FBCs was observed in the original scaffold localization of the La2 scaffolds after 24 and 36 weeks, partially surrounded by fibrous tissue. Only a moderate number of fibrocytes occurred in the granulation tissue of the LAE442 scaffolds, but there was no capsule formation. In comparison, the La2 scaffolds in the present study showed an overly rapid degradation, associated with a distinct fibrous capsule formation after 6 and 12 weeks. This formation of a fibrous capsule around a biomaterial is induced by the body to protect the surrounding host tissue [4]. Furthermore, in the present study, the increased accumulation of gas around the La2 scaffolds may also have influenced the extent of capsule formation. According to the study by Nuss *et al*, the combination of a thick fibrous capsule and a high number of macrophages and FBCs indicates insufficient biocompatibility [4], as can be assumed for the La2 scaffolds.

In addition, the EDX analysis in the area of these cell clusters (macrophages and FBCs), which were observed in La2 scaffolds after 36 weeks, showed an increased concentration of lanthanum of up to 67.3 wt.%. Free lanthanides have an affinity to accumulate in the bone due to their similar physicochemical properties to calcium [61]. A progressive loss of membrane integrity in macrophages was observed in the *in vitro* study by Southwick *et al* after exposure to lanthanum [62]. Feyerabend *et al* reported a reduction in cell viability of the macrophage cell line RAW 264.7 after a lanthanum exposure time of 24 h [63]. Thus, the large clusters of macrophages and FBCs in the original scaffold localization of La2 could probably be associated with apoptosis of these cells due to the lanthanum accumulation.

Furthermore, the MgF_2 coating was investigated by means of EDX analysis. In the present study, about 2/3 of the original fluoride disappeared from the scaffold surface after 6 weeks and hardly any fluoride could be detected after 12 weeks. In contrast, Witte *et al* described less than 1 wt.% fluoride on the implant surface after only 4 weeks and thus a complete disappearance of the initial MgF_2 coating (thickness 150–200 μm) on the LAE442 implants [29]. Despite the same alloy and coating manufacturing process, fluoride lasted longer in the present study than by Witte *et al*, although the initial coating was much thinner. Subsequent studies with more frequent investigation time points would be necessary to accurately evaluate the reduction of corrosion provided by the MgF_2 coating.

The EDX analysis of the LAE442 scaffolds showed both an accumulation of calcium and phosphorus in the degradation layer and a deposition of both elements on the scaffold surface, as already described earlier [2]. This fact could explain the increasing density of the LAE442 scaffolds observed in

μ CT80 over time. In many other *in vivo* studies, this accumulation of a mineralized phase of calcium and phosphorus in the degradation layer of magnesium implants has been observed [30, 35, 64]. In the present study, these deposits of calcium and phosphorus on the LAE442 scaffolds showed direct contact to the surrounding bone, also described by Witte *et al* for porous AZ91D scaffolds in a rabbit model [13].

5. Conclusion

In summary, the present study showed an inhomogeneous and fast degradation for La2. In addition, the La2 scaffolds exhibited an inadequate osseointegration with fibrous capsule formation in the early implantation periods and a foreign body reaction at later implantation periods. LAE442, on the other hand, showed direct bone-to scaffold contact, a homogeneous degradation behaviour and almost maintained its original shape up to 36 weeks. Within the pores of the LAE442 scaffolds vascularization, moderate cellular response, as well as granulation tissue and bone were observed at all implantation periods. Furthermore, osteoid-like bone matrix was detected on the scaffold surface and within the pores of LAE442. Based on the results of this study, porous LAE442 showed promise as degradable scaffolds for bone defect repair in terms of degradation behaviour and biocompatibility. However, further studies are needed to show it would have the necessary mechanical properties required over time for weight-bearing bone defects. Moreover, additional coatings (for example CaP) could further delay the degradation rate and gas production and might have a positive effect on the mineralisation of the osteoid-like bone matrix.

Data availability statement

The data that support the findings of this study are available upon reasonable request from the authors.

Acknowledgments

The authors gratefully acknowledge the financial support by the German Research Foundation (DFG) within the project ‘Interfacial effects and integration behaviour of magnesium-based sponges as bioresorbable bone substitute material’ (Funding Number 271761343). Furthermore, the authors thank Lisa Wurm and Beatrix Limmer for their excellent technical support, Yury Zablotiski for his help with the statistical analysis and Brigitte von Rechenberg for her input regarding the histological evaluation.

ORCID iD

N Kleer-Reiter  <https://orcid.org/0000-0002-6853-9040>

References

- [1] Liang H, Li X, Shimer A L, Balian G and Shen F H 2014 A novel strategy of spine defect repair with a degradable bioactive scaffold preloaded with adipose-derived stromal cells *Spine J.* **14** 445–54
- [2] Maier H J, Julmi S, Behrens S, Klose C, Gartzke A-K, Wriggers P, Waselau A-C and Meyer-Lindenberg A 2020 Magnesium alloys for open-pored bioresorbable implants *JOM* **72** 1859–69
- [3] de Long W G Jr, Einhorn T A, Koval K, McKee M, Smith W, Sanders R and Watson T 2007 Bone grafts and bone graft substitutes in orthopaedic trauma surgery. A critical analysis *J. Bone Joint Surg. Am.* **89** 649–58
- [4] Nuss K M and von Rechenberg B 2008 Biocompatibility issues with modern implants in bone—a review for clinical orthopedics *Open Orthop. J.* **2** 66–78
- [5] Karageorgiou V and Kaplan D 2005 Porosity of 3D biomaterial scaffolds and osteogenesis *Biomaterials* **26** 5474–91
- [6] Yazdimamaghani M, Razavi M, Vashae D, Moharamzadeh K, Boccaccini A R and Tayebi L 2017 Porous magnesium-based scaffolds for tissue engineering *Mater. Sci. Eng. C* **71** 1253–66
- [7] Bobe K, Willbold E, Morgenthal I, Andersen O, Studnitzky T, Nellesen J, Tillmann W, Vogt C, Vano K and Witte F 2013 *In vitro* and *in vivo* evaluation of biodegradable, open-porous scaffolds made of sintered magnesium W4 short fibres *Acta Biomater.* **9** 8611–23
- [8] Klenke F M, Liu Y, Yuan H, Hunziker E B, Siebenrock K A and Hofstetter W 2008 Impact of pore size on the vascularization and osseointegration of ceramic bone substitutes *in vivo J. Biomed. Mater. Res. A* **85** 777–86
- [9] Mavrogenis A F, Dimitriou R, Parvizi J and Babis G C 2009 Biology of implant osseointegration *J. Musculoskelet. Neuronal Interact.* **9** 61–71
- [10] Bohner M, Baroud G, Bernstein A, Doebelin N, Galea L, Hesse B, Heuberger R, Meille S, Michel P and von Rechenberg B 2017 Characterization and distribution of mechanically competent mineralized tissue in micropores of β -tricalcium phosphate bone substitutes *Mater. Today* **20** 106–15
- [11] von Doernberg M C, von Rechenberg B, Bohner M, Grunenfelder S, van Lenthe G H, Muller R, Gasser B, Mathys R, Baroud G and Auer J 2006 *In vivo* behavior of calcium phosphate scaffolds with four different pore sizes *Biomaterials* **27** 5186–98
- [12] Dorozhkin S V 2010 Bioceramics of calcium orthophosphates *Biomaterials* **31** 1465–85
- [13] Witte F, Kaese V, Haferkamp H, Switzer E, Meyer-Lindenberg A, Wirth C J and Windhagen H 2005 *In vivo* corrosion of four magnesium alloys and the associated bone response *Biomaterials* **26** 3557–63
- [14] Ayvaz M, Bekmez S, Yucekul A, Mermerkaya M U and Tokgozoglu A M 2018 Titanium mesh cage as an alternative reconstruction method for epiphyseal-sparing tumour resections in children *J. Pediatr. Orthop. B* **27** 350–5
- [15] Segal U and Shani J 2010 Surgical management of large segmental femoral and radial bone defects in a dog: through use of a cylindrical titanium mesh cage and a cancellous bone graft *Vet. Comp. Orthop. Traumatol.* **23** 66–70
- [16] Nagels J, Stokdijk M and Rozing P M 2003 Stress shielding and bone resorption in shoulder arthroplasty *J. Shoulder Elbow Surg.* **12** 35–39

- [17] Staiger M P, Pietak A M, Huadmai J and Dias G 2006 Magnesium and its alloys as orthopedic biomaterials: a review *Biomaterials* **27** 1728–34
- [18] Willbold E et al 2013 Biocompatibility of rapidly solidified magnesium alloy RS66 as a temporary biodegradable metal *Acta Biomater.* **9** 8509–17
- [19] Vormann J 2003 Magnesium: nutrition and metabolism *Mol. Aspects Med.* **24** 27–37
- [20] Song G and Atrens A 2003 Understanding magnesium corrosion—a framework for improved alloy performance *Adv. Eng. Mater.* **5** 837–58
- [21] Janning C, Willbold E, Vogt C, Nellesen J, Meyer-Lindenberg A, Windhagen H, Thorey F and Witte F 2010 Magnesium hydroxide temporarily enhancing osteoblast activity and decreasing the osteoclast number in peri-implant bone remodelling *Acta Biomater.* **6** 1861–8
- [22] Witte F, Hort N, Vogt C, Cohen S, Kainer K U, Willumeit R and Feyerabend F 2008 Degradable biomaterials based on magnesium corrosion *Curr. Opin. Solid State Mater. Sci.* **12** 63–72
- [23] Willbold E et al 2015 Effect of the addition of low rare earth elements (lanthanum, neodymium, cerium) on the biodegradation and biocompatibility of magnesium *Acta Biomater.* **11** 554–62
- [24] Acar B, Kose O, Unal M, Turan A, Kati Y A and Guler F 2020 Comparison of magnesium versus titanium screw fixation for biplane chevron medial malleolar osteotomy in the treatment of osteochondral lesions of the talus *Eur. J. Orthop. Surg. Traumatol.* **30** 163–73
- [25] Atkinson H D, Khan S, Lashgari Y and Ziegler A 2019 Hallux valgus correction utilising a modified short scarf osteotomy with a magnesium biodegradable or titanium compression screws—a comparative study of clinical outcomes *BMC Musculoskelet. Disorders* **20** 334
- [26] Angrisani N, Reifenrath J, Zimmermann F, Eifler R, Meyer-Lindenberg A, Vano-Herrera K and Vogt C 2016 Biocompatibility and degradation of LAE442-based magnesium alloys after implantation of up to 3.5 years in a rabbit model *Acta Biomater.* **44** 355–65
- [27] Krause A, von der Höh N, Bormann D, Krause C, Bach F-W, Windhagen H and Meyer-Lindenberg A 2010 Degradation behaviour and mechanical properties of magnesium implants in rabbit tibiae *J. Mater. Sci.* **45** 624–32
- [28] Thomann M, Krause C, Bormann D, von der Höh N, Windhagen H and Meyer-Lindenberg A 2009 Comparison of the resorbable magnesium alloys LAE442 und MgCa_{0.8} concerning their mechanical properties, their progress of degradation and the bone-implant-contact after 12 months implantation duration in a rabbit model *Materwiss. Werksttech.* **40** 82–7
- [29] Witte F, Fischer J, Nellesen J, Vogt C, Vogt J, Donath T and Beckmann F 2010 *In vivo* corrosion and corrosion protection of magnesium alloy LAE442 *Acta Biomater.* **6** 1792–9
- [30] Ullmann B, Reifenrath J, Seitz J M, Bormann D and Meyer-Lindenberg A 2013 Influence of the grain size on the *in vivo* degradation behaviour of the magnesium alloy LAE442 *Proc. Inst. Mech. Eng. H* **227** 317–26
- [31] Hamp C, Angrisani N, Reifenrath J, Bormann D, Seitz J M and Meyer-Lindenberg A 2013 Evaluation of the biocompatibility of two magnesium alloys as degradable implant materials in comparison to titanium as non-resorbable material in the rabbit *Mater. Sci. Eng. C* **33** 317–26
- [32] Weizbauer A, Seitz J M, Werle P, Hegermann J, Willbold E, Eifler R, Windhagen H, Reifenrath J and Waizy H 2014 Novel magnesium alloy Mg–2La caused no cytotoxic effects on cells in physiological conditions *Mater. Sci. Eng. C* **41** 267–73
- [33] Lalk M, Reifenrath J, Angrisani N, Bondarenko A, Seitz J M, Mueller P P and Meyer-Lindenberg A 2013 Fluoride and calcium-phosphate coated sponges of the magnesium alloy AX30 as bone grafts: a comparative study in rabbits *J. Mater. Sci. Mater. Med.* **24** 417–36
- [34] Fischerauer S F, Kraus T, Wu X, Tangl S, Sorantin E, Hanzi A C, Löffler J F, Uggowitzer P J and Weinberg A M 2013 *In vivo* degradation performance of micro-arc-oxidized magnesium implants: a micro-CT study in rats *Acta Biomater.* **9** 5411–20
- [35] Thomann M, Krause C, Angrisani N, Bormann D, Hassel T, Windhagen H and Meyer-Lindenberg A 2010 Influence of a magnesium-fluoride coating of magnesium-based implants (MgCa_{0.8}) on degradation in a rabbit model *J. Biomed. Mater. Res. A* **93** 1609–19
- [36] Yu W et al 2017 *In vitro* and *in vivo* evaluation of MgF₂ coated AZ31 magnesium alloy porous scaffolds for bone regeneration *Colloids Surf. B* **149** 330–40
- [37] Zhao N, Workman B and Zhu D 2014 Endothelialization of novel magnesium–rare earth alloys with fluoride and collagen coating *Int. J. Mol. Sci.* **15** 5263–76
- [38] Li Z, Shizhao S, Chen M, Fahlman B D, Debaio L and Bi H 2017 *In vitro* and *in vivo* corrosion, mechanical properties and biocompatibility evaluation of MgF₂-coated Mg–Zn–Zr alloy as cancellous screws *Mater. Sci. Eng. C* **75** 1268–80
- [39] Seyedraoufi Z S and Mirdamadi S 2013 Synthesis, microstructure and mechanical properties of porous Mg–Zn scaffolds *J. Mech. Behav. Biomed. Mater.* **21** 1–8
- [40] Witte F, Ulrich H, Palm C and Willbold E 2007 Biodegradable magnesium scaffolds: part II: peri-implant bone remodeling *J. Biomed. Mater. Res. A* **81** 757–65
- [41] Julmi S, A-k K, Waselau A-C, Meyer-Lindenberg A, Wriggers P, Klose C and Maier H J 2019 Processing and coating of open-pored absorbable magnesium-based bone implants *Mater. Sci. Eng. C* **98** 1073–86
- [42] Julmi S, Klose C, Krüger A-K, Wriggers P and Maier H J 2017 Development of sponge structure and casting conditions for absorbable magnesium bone implants *TMS 2017 146th Annual Meeting & Exhibition Supplemental Proc.* (Springer, Cha) pp 307–17
- [43] Kleer N, Julmi S, Gartzke A-K, Augustin J, Feichtner F, Waselau A-C, Klose C, Maier H, Wriggers P and Meyer-Lindenberg A J M 2019 Comparison of degradation behaviour and osseointegration of the two magnesium scaffolds, LAE442 and La2, *in vivo* *Materialia* **8** 100436
- [44] Lalk M, Reifenrath J, Rittershaus D, Bormann D and Meyer-Lindenberg A 2010 Biocompatibility and degradation behaviour of degradable magnesium sponges coated with bioglass—method establishment within the framework of a pilot study *Materwiss. Werksttech.* **41** 1025–34
- [45] Donath K and Breuner G 1982 A method for the study of undecalcified bones and teeth with attached soft tissues. The Sage-Schliff (sawing and grinding) technique *J. Oral Pathol.* **11** 318–26
- [46] Huehnerschulte T A, Reifenrath J, von Rechenberg B, Dziuba D, Seitz J M, Bormann D, Windhagen H and Meyer-Lindenberg A 2012 *In vivo* assessment of the host reactions to the biodegradation of the two novel magnesium alloys ZEK100 and AX30 in an animal model *Biomed. Eng. Online* **11** 14
- [47] Cheng M Q, Wahafu T, Jiang G F, Liu W, Qiao Y Q, Peng X C, Cheng T, Zhang X L, He G and Liu X Y 2016 A novel open-porous magnesium scaffold with controllable microstructures and properties for bone regeneration *Sci. Rep.* **6** 24134
- [48] Mousny M, Omelon S, Wise L, Everett E T, Dumitriu M, Holmyard D P, Banse X, Devogelaer J P and Grynypas M D 2008 Fluoride effects on bone formation and mineralization are influenced by genetics *Bone* **43** 1067–74
- [49] Hamp C, Ullmann B, Reifenrath J, Angrisani N, Dziuba D, Bormann D, Seitz J M and Meyer-Lindenberg A 2012 Research on the biocompatibility of the new magnesium alloy LANd442—an *in vivo* study in the rabbit tibia over 26 weeks *Adv. Eng. Mater.* **14** B28–B37
- [50] Erdmann N, Angrisani N, Reifenrath J, Lucas A, Thorey F, Bormann D and Meyer-Lindenberg A 2011 Biomechanical testing and degradation analysis of MgCa_{0.8} alloy screws: a comparative *in vivo* study in rabbits *Acta Biomater.* **7** 1421–8

- [51] Jansen J A, Dhert W J, van der Waerden J P and von Recum A F 1994 Semi-quantitative and qualitative histologic analysis method for the evaluation of implant biocompatibility *J. Invest. Surg.* **7** 123–34
- [52] Hofmann S et al 2013 Remodeling of tissue-engineered bone structures *in vivo Eur. J. Pharm. Biopharm.* **85** 119–29
- [53] von der Höh N, Bormann D, Lucas A, Denkena B, Hackenbroich C and Meyer-Lindenberg A 2009 Influence of different surface machining treatments of magnesium-based resorbable implants on the degradation behavior in rabbits *J. Adv. Eng. Mater.* **11** B47–B54
- [54] Rossig C, Angrisani N, Helmecke P, Besdo S, Seitz J M, Welke B, Fedchenko N, Kock H and Reifenrath J 2015 *In vivo* evaluation of a magnesium-based degradable intramedullary nailing system in a sheep model *Acta Biomater.* **25** 369–83
- [55] Payr E 1900 Beiträge zur Technik der Blutgefäß- und Nervennaht nebst Mittheilungen über die Verwendung eines resorbirbaren Metalles in der Chirurgie *Arch. Klin. Chir.* **62** 67–93
- [56] Kraus T et al 2014 Biodegradable Fe-based alloys for use in osteosynthesis: outcome of an *in vivo* study after 52 weeks *Acta Biomater.* **10** 3346–53
- [57] Kraus T, Fischerauer S, Treichler S, Martinelli E, Eichler J, Myrissa A, Zotsch S, Uggowitz P J, Löffler J F and Weinberg A M 2018 The influence of biodegradable magnesium implants on the growth plate *Acta Biomater.* **66** 109–17
- [58] Sedman A B, Alfrey A C, Miller N L and Goodman W G 1987 Tissue and cellular basis for impaired bone formation in aluminum-related osteomalacia in the pig *J. Clin. Invest.* **79** 86–92
- [59] Talwar H S, Reddi A H, Menczel J, Thomas W C Jr and Meyer J L 1986 Influence of aluminum on mineralization during matrix-induced bone development *Kidney Int.* **29** 1038–42
- [60] Quarles L D, Dennis V W, Gitelman H J, Harrelson J M and Drezner M K 1985 Aluminum deposition at the osteoid-bone interface. An epiphenomenon of the osteomalacic state in vitamin D-deficient dogs *J. Clin. Invest.* **75** 1441–7
- [61] Li W P, Ma D S, Higginbotham C, Hoffman T, Ketring A R, Cutler C S and Jurisson S S 2001 Development of an *in vitro* model for assessing the *in vivo* stability of lanthanide chelates *Nucl. Med. Biol.* **28** 145–54
- [62] Southwick F S, Li W, Zhang F, Zeile W L and Purich D L 2003 Actin-based endosome and phagosome rocketing in macrophages: activation by the secretagogue antagonists lanthanum and zinc *Cell Motil. Cytoskeleton* **54** 41–55
- [63] Feyerabend F, Siemers C, Willumeit R and Rosler J 2009 Cytocompatibility of a free machining titanium alloy containing lanthanum *J. Biomed. Mater. Res. A* **90** 931–9
- [64] von der Höh N, von Rechenberg B, Bormann D, Lucas A and Meyer-Lindenberg A 2009 Influence of different surface machining treatments of resorbable magnesium alloy implants on degradation—EDX-analysis and histology results *Mat.-wiss. Werkstofftech.* **40** 88–93